Imaging the He_2 quantum halo state using a free electron laser

Stefan Zeller[a,1], Maksim Kunitski[a], Jörg Voigtsberger[a], Anton Kalinin[a], Alexander Schottelius[a], Carl Schober[a], Markus Waitz[a], Hendrik Sann[a], Alexander Hartung[a], Tobias Bauer[a], Martin Pitzer[a], Florian Trinter[a], Christoph Goihl[a], Christian Janke[a], Martin Richter[a], Gregor Kastirke[a], Miriam Weller[a], Achim Czasch[a], Markus Kitzler[b], Markus Braune[c], Robert E. Grisenti[a,d], Wieland Schöllkopf[e], Lothar Ph. H. Schmidt[a], Markus S. Schöffler[a], Joshua B. Williams[f], Till Jahnke[a], and Reinhard Dörner[a,1]

[a]Institut für Kernphysik, Goethe-Universität Frankfurt, 60438 Frankfurt, Germany; [b]Photonics Institute, Vienna University of Technology, 1040 Vienna, Austria; [c]Deutsches Elektronen-Synchrotron, 22607 Hamburg, Germany; [d]GSI Helmholtz Centre for Heavy Ion Research, 64291 Darmstadt, Germany; [e]Department of Molecular Physics, Fritz-Haber-Institut, 14195 Berlin, Germany; and [f]Department of Physics, University of Nevada, Reno, NV 89557

Edited by Marlan O. Scully, Texas A&M University, College Station, TX, and approved November 3, 2016 (received for review June 30, 2016)

Quantum tunneling is a ubiquitous phenomenon in nature and crucial for many technological applications. It allows quantum particles to reach regions in space which are energetically not accessible according to classical mechanics. In this "tunneling region," the particle density is known to decay exponentially. This behavior is universal across all energy scales from nuclear physics to chemistry and solid state systems. Although typically only a small fraction of a particle wavefunction extends into the tunneling region, we present here an extreme quantum system: a gigantic molecule consisting of two helium atoms, with an 80% probability that its two nuclei will be found in this classical forbidden region. This circumstance allows us to directly image the exponentially decaying density of a tunneling particle, which we achieved for over two orders of magnitude. Imaging a tunneling particle shows one of the few features of our world that is truly universal: the probability to find one of the constituents of bound matter far away is never zero but decreases exponentially. The results were obtained by Coulomb explosion imaging using a free electron laser and furthermore yielded He_2's binding energy of 151.9 ± 13.3 neV, which is in agreement with most recent calculations.

clusters | helium dimer | wavefunction | tunneling

Attractive forces allow particles to condense into stable bound systems such as molecules or nuclei with a ground state and (in most cases) energetically excited bound states, as shown in Fig. 1. Classical particles situated in such a binding potential oscillate back and forth between two turning points. The regions beyond these points are inaccessible for a classical particle due to a lack of energy. Quantum particles, however, can penetrate into the potential barrier by a phenomenon known as "tunneling." Tunneling is omnipresent in nature and occurs on all energy scales from megaelectron volts in nuclear physics to electron volts in molecules and solids and to nanoelectron volts in optical lattices. For bound matter, the fraction of the probability density distribution in this classically forbidden region is usually small. For shallow short-range potentials, this situation can change dramatically: upon decreasing the potential depth, excited states are expelled one after the other as they become unbound (transition from *A* to *B* in Fig. 1). A further decrease of the potential depth effects the ground state as well, as more and more of its wavefunction expands into the tunneling region (Fig. 1 *C* and *D*). Consequently, at the threshold (i.e., in the limit of vanishing binding energy), the size of the quantum system expands to infinity. For short-range potentials, this expansion is accompanied by the fact that the system becomes less "classical" and more quantum-like. Systems existing near that threshold (and therefore being dominated by the tunneling part of their wavefunction) are called "quantum halo states" (1). These states are known, for example, from nuclear physics where ^{11}Be and ^{11}Li form halo states (2–4).

One of the most extreme examples of such a quantum halo state can be found in the realm of atomic physics: the helium dimer (He_2). The dimer is bound by only the van der Waals force, and the He–He interaction potential (Fig. 1*D*) has a minimum of about 1 meV at an internuclear distance of about 3 Å [0.947 meV/2.96 Å (5)]. For a long time, it was controversial whether the zero-point energy of the helium dimer is already larger than the depth of the potential well and thus whether the helium dimer exists as a stable molecule at all. Although ^{3}He^{4}He is indeed unbound because of its bigger zero-point energy, stable $^4He_2$ was finally found experimentally in 1993 and 1994 (6, 7). It turns out that He_2 has no bound excited rotational states because the centrifugal force associated with $1\hbar$ of angular momentum already leads to dissociation. Experiments using matter wave diffraction confirmed the halo character of He_2 by measuring a mean value of the internuclear distance of 52 Å (8). This result is in agreement with some theoretical predictions but in conflict with the most recent calculations (5). Resolving this conflict is also of importance for the planned redefinition of the Kelvin unit of thermodynamic temperature in terms of the Boltzmann constant (9). Thermometry today uses theoretical values for the thermal conductivity and viscosity of helium. Those properties are based on the same He–He interaction potential used to calculate the He_2 binding energy, which was shown to be incompatible

Significance

In bound matter on all length scales, from nuclei to molecules to macroscopic solid objects, most of the density of the bound particles is within the range of the interaction potential which holds the system together. Quantum halos on the contrary are a type of matter where the particle density is mostly outside the range of the interaction potential in the tunneling region of the potential. Few examples of these fascinating systems are known in nuclear and molecular physics. The conceptually simplest halo system is made of only two particles. Here we experimentally image the wavefunction of the He_2 quantum halo. It shows the predicted exponential shape of a tunneling wavefunction.

Author contributions: S.Z., M. Kunitski, J.V., R.E.G., L.Ph.H.S., M.S.S., T.J., and R.D. designed research; S.Z., M. Kunitski, J.V., A.K., A.S., C.S., M. Waitz, H.S., A.H., T.B., M.P., F.T., C.G., C.J., M.R., G.K., M. Weller, M. Kitzler, M.B., L.Ph.H.S., M.S.S., J.B.W., T.J., and R.D. performed research; M.B. provided extensive support as a beamline scientist; S.Z., M. Kunitski, J.V., A.K., T.B., A.C., W.S., T.J., and R.D. contributed new reagents/analytic tools; S.Z., T.J., and R.D. analyzed data; and S.Z., M. Kunitski, J.B.W., T.J., and R.D. wrote the paper.

The authors declare no conflict of interest.

This article is a PNAS Direct Submission.

[1]To whom correspondence may be addressed. Email: zeller@atom.uni-frankfurt.de or doerner@atom.uni-frankfurt.de.

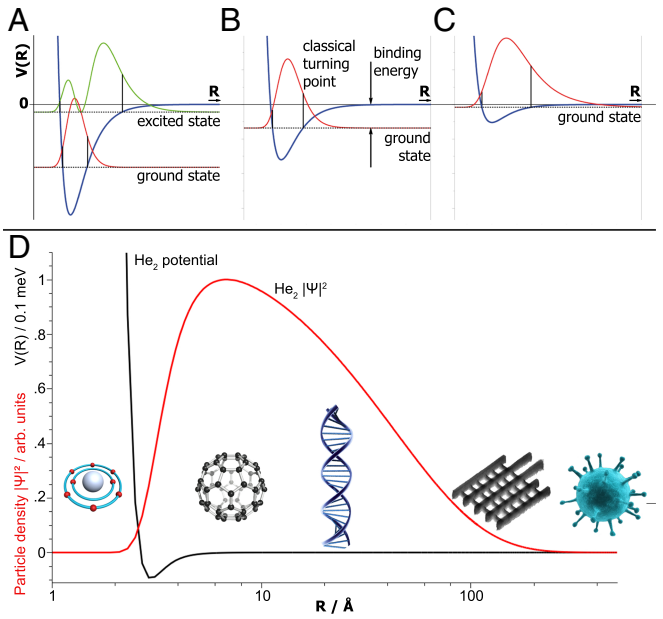

Fig. 1. (*A*) Shallow short-range potential holding a ground and an excited state. As the potential depth decreases (*B*), the excited state becomes unbound, leaving only the ground state. Further decrease (*C*) leads to the particle probability density distribution leaking more into the classically forbidden region. In the extreme case of the helium dimer (note the logarithmic *R* scale) (*D*), this effect allows the wavefunction to extend to sizes of fullerenes, the diameter of DNA, and even small viruses (He_2 potential and wavefunction taken from ref. 5), whereas the classical turning point is located at 13.6 Å, and the overall wavefunction extends to more than 200 Å.

with previous experiments (8, 10) (see ref. 11 for a more detailed discussion).

At the same time, its quantum halo character makes He_2 a prime candidate for visualizing the predicted universal exponential decrease of a tunneling wavefunction in an experiment by triggering a Coulomb explosion with a free electron laser (FEL).

Results

In the corresponding experiment presented here, helium clusters were produced by expanding cooled helium gas through a 5μm nozzle. By matter wave diffraction, a pure helium-dimer beam was separated from the lighter monomers and heavier clusters (6). In two experimental campaigns, both atoms of the dimer were then singly ionized using either single-photon ionization using photons provided by a FEL [<100 fs, 18.5 nm; Freie–Elektronen Laser in Hamburg (FLASH)] or tunnel ionization using a strong ultrashort laser field (Ti:Sa laser; 780 nm; Dragon KMLabs). In both cases, the ionization of the two atoms occurs fast compared with the nuclear motion, thus triggering an instantaneous Coulomb explosion of the repelling ionized particles. The Coulomb explosion converts the potential energy of the two ions located at an internuclear distance R into a released kinetic energy (KER) according to

$$R = \frac{1}{KER}. \qquad [1]$$

By recording a large number of Coulomb explosion events, via cold target recoil ion momentum spectroscopy (COLTRIMS) (12–14), a distribution of measured distances R (as shown in Fig. 2*A*) is obtained. This distribution represents a direct measurement of the square of the helium-dimer wavefunction $|\Psi|^2$. The classically allowed part of $|\Psi|^2$ provides a cross-check for our measurement because it falls off steeply at the inner turning point of the helium-dimer potential and theoretical calculations agree well on the location of the turning point. A comparison of our measured probability density distribution close to the inner turning point and some theoretical predictions are shown in Fig. 2*B*. Here, two exemplary theoretical curves (5, 15) are depicted along with a measurement conducted at our Ti:Sa laser because it provides very high resolution and statistics for small internuclear distances.

The classically forbidden part of $|\Psi|^2$ is shown in Fig. 2*C* on a logarithmic scale. For internuclear distances larger than 30 Å, the helium-dimer potential is two orders of magnitude smaller than the predicted ground-state binding energy and thus can safely be approximated to zero. Accordingly, the wavefunction is approximated in this region by the solution of the Schrödinger equation below a step-like barrier, which is given by

$$\Psi(R) \propto e^{-\sqrt{\frac{2m}{\hbar^2}E_{bind}}R}. \qquad [2]$$

Because the mass m and Planck's constant $\hbar$ are fixed, the only variable defining the slope of the exponential decay is the binding energy E_{bind}. Therefore, the binding energy can be extracted from the measurement by an exponential fit to the pair-distance distribution, as depicted in Fig. 2*C*. From the fit, we obtain a helium-dimer binding energy of 151.9 ± 13.3 neV (see *Materials and Methods* for a discussion of errors and corrections to Eq. **2**). This value can be used for a fully experimental determination of the binding energy of the helium-trimer Efimov state, which was discovered recently using the same experimental setup (16).

Discussion

The theoretical value for the binding energy was under dispute for many years (17–20). Predictions range from 44.8 neV (18) to 161.7 neV (21). Recently calculations became available that include quantum electrodynamical effect and relativistic effects and go beyond the Born Oppenheimer approximation. These supposedly most precise calculations predict a binding energy of 139.2 ± 2.9 neV (5), which is in disagreement with the most recent experimental value of 94.8 + 25.9/-17.2 neV obtained in pioneering experiments by evaluating matter wave diffraction patterns and relying on a detailed theoretical modeling of the interaction of the dimer with the grating surface (8). The present value of 151.9 ± 13.3 neV is in good agreement with the prediction of Przybytek et al. (5) (139.2 ± 2.9 neV) and in clear disagreement with the predictions from some He–He interaction potentials, including the popular Tang–Toennies–Yiu potential (TTY) (19) and the mimic of the Liu–McLean potential (LM2M2) (22) yielding 114 and 113 neV, respectively.

The helium dimer is a remarkable example of a system existing predominantly in the quantum mechanical tunneling regime. We were able to reveal the full shape of the wavefunction experimentally. The measured data confirm the universal exponential behavior of wavefunctions under a potential barrier on unprecedented scales and yield a revised experimental value for the binding energy of the helium dimer, which has been under dispute for more than 20 y.

Materials and Methods

Dimer Preparation and Detection. A mixture of helium clusters was produced by expanding gaseous helium through a 5 μm nozzle. The nozzle was cooled down to 8 K, and a driving pressure of 450 hPa absolute pressure was applied to maximize the dimer content in the molecular beam (16). To obtain a pure helium-dimer target beam, we made use of matter wave diffraction. All clusters have the same velocity but can be sorted by mass because their diffraction angle behind a transmission grating (100-nm period) depends on their de Broglie wavelengths ($\lambda = h/mv$, with Planck's constant h, mass m, and velocity v). That way, only dimers reach the laser focus, whereas the dominant fraction of atomic helium, as well as the

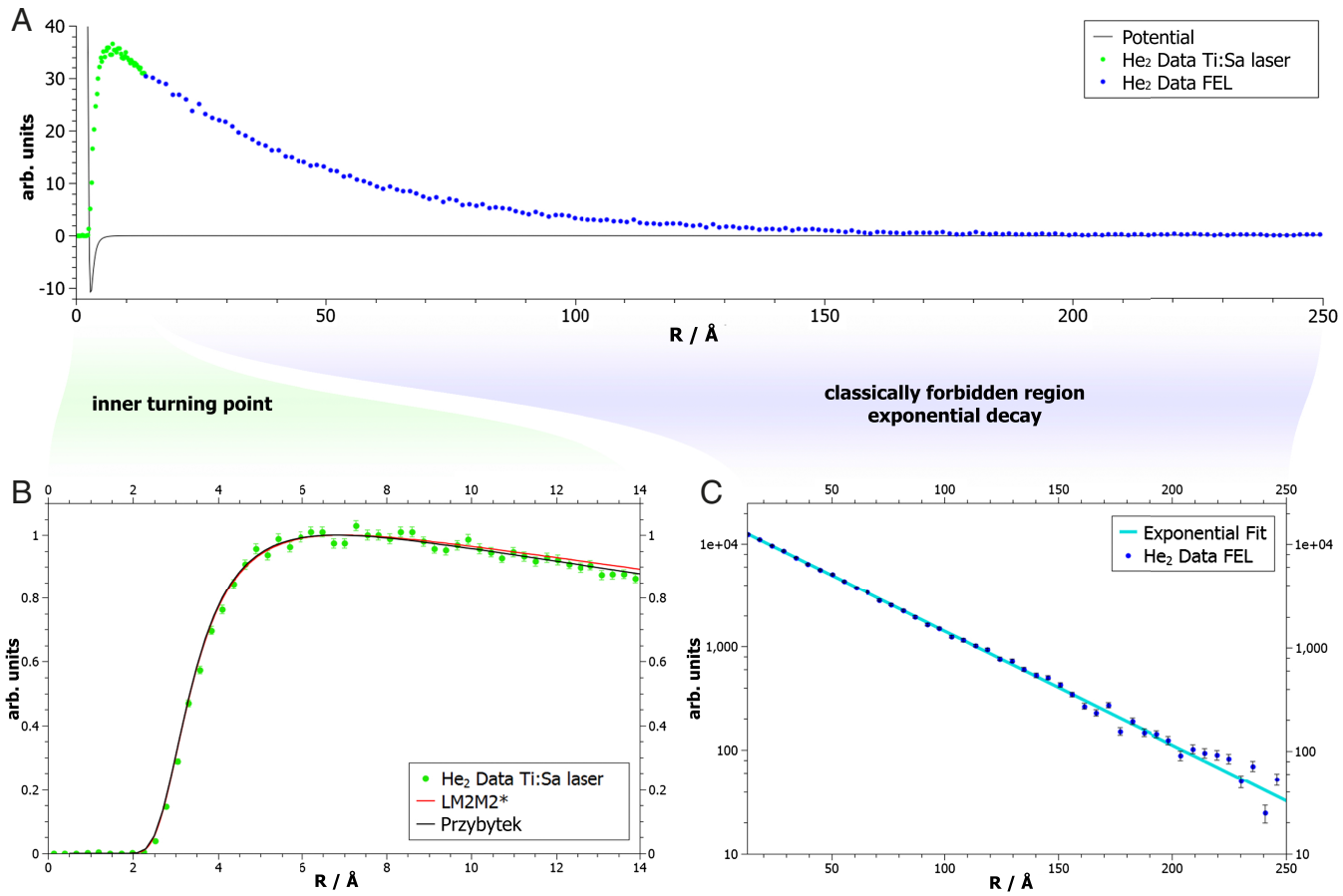

Fig. 2. (*A*) Measurement of the helium-dimer wavefunction. (*B* and *C*) Two detailed views show the important features of this quantum system: the region of the inner turning point (*B*) is in agreement with theoretical predictions LM2M2* (15) and Przybytek et al. (5), and the exponential decay in the classic forbidden region (*C*). A helium-dimer binding energy of 151.9 ± 13.3 neV is obtained from the exponential slope. The electron recoil has to be taken into account to conclude from the slope shown in *C* to the value of the binding energy (see *Materials and Methods* for details).

share of helium trimers, present at the chosen gas expansion conditions get deflected away from the ionization region. Fig. 3 shows a schematic of the setup.

The two atoms constituting the dimer get singly ionized in the focus either via photoeffect (FEL; 18.5 nm; FLASH) or via tunnel ionization (Ti:Sa laser; 780 nm; Dragon KMLabs). The two positively charged ions repel each other, resulting in a Coulomb explosion. The ionic momenta acquired in this explosion were measured by COLTRIMS. A homogeneous electric field of 4.41 V/cm (at FEL) and 3.09 V/cm (at Ti:Sa laser) guides the ions to the detector, which measures time-of-flight and position of impact using microchannel plates (MCPs) and delay line anodes (12). With known electric fields, ion masses, ion charges, and a distance from focus to detector of 39 mm, the initial momentum vector of the ions, and thus the KER, can be reconstructed.

Detector Calibration. The binding energy of the helium dimer is derived from the measured KER. Therefore, a precise energy calibration is needed. The crucial parameters for this calibration are the absolute value of the electric field in the spectrometer and the position calibration of the detector. The electric field was obtained by measuring the kinetic energy release spectrum of the N_2 breakup, which provides very narrow peaks. Transitions from $D^3\Pi g$ and $D^1\Sigma u^+$ into continuum could be identified and met reference measurements (23), with a mean relative deviation of 0.054%. This measurement yielded the calibration of the momentum component along the time-of-flight direction of the spectrometer.

The position calibration was done by comparing the momentum component in the time-of-flight direction with the ones perpendicular to it. For this purpose, we performed two calibration measurements with isotropic dissociation channels (N_2O/Ne_2). Most relevant, due to energetic proximity to the helium-dimer breakup, is the N_2O channel at 0.16 eV KER, with a mean relative deviation of 6.2%, whereas additional channels yield a smaller deviation, with 0.62% (N_2O at 0.36 eV) and 0.15% (Ne_2 at 4.4 eV).

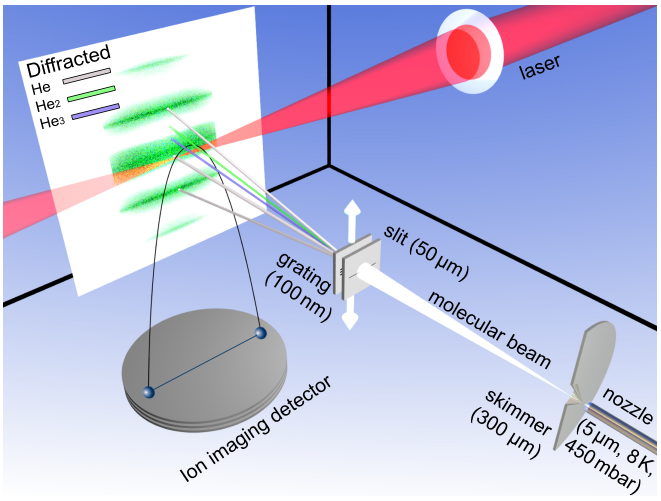

Fig. 3. Overlap between laser focus and a pure helium-dimer beam, created by a molecular beam diffracted at a nanograting. Distances between the beam elements were as follows: nozzle to skimmer, 14 mm; skimmer to slit, 332 mm; slit to grating, 30 mm; and grating to focus, 491 mm. The focus diameter was about 20 µm.

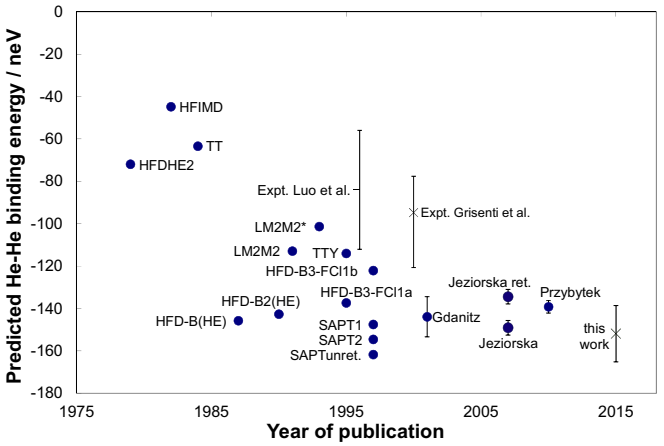

Fig. 4. The predicted values for the helium-dimer binding energy using various theoretical calculations [HFDHE2 (Hartree–Fock dispersion for He_2) (17), HFIMD (Hartree–Fock with intraatomic correlation correction and model dispersion) (18), TT (Tang–Toennies) (26), HFD-B(HE) (Hartree–Fock plus damped dispersion B for helium) (27), HFD-B2 (Hartree–Fock plus dispersion B2) (28), LM2M2 (22), LM2M2* (15), TTY (19), HFD-B3-FCI1a (Hartree-Fock-dispersion B3 full configuration interaction) (29), HFD-B3-FCI1b, SAPT (symmetry-adapted perturbation theory) (21, 30), Gdanitz (20), Jeziorska et al. (31), and Przybytek et al. (5)] are displayed alongside experimental measurements from Luo et al. (10), Grisenti et al. (8), and the present work.

For the experiment at FLASH, despite excellent vacuum conditions ($8{\cdot}10^{-12}$ hPa), an average of about 50 ions were collected for every FEL pulse. The majority of ions were charged hydrogen atoms or molecules with short times-of-flight, which could be gated out by software during data acquisition before writing to the hard drive. Nevertheless, the MCPs endured constant stress, which led to a drop in detection efficiency in the center of the detector. The detection efficiency was corrected to its normal level using a residual gas calibration measurement with a Gaussian-shaped correction function containing a 5.5% uncertainty. This uncertainty leads to an error of ± 1 neV on the binding energy. In addition, random coincidences from ionizations of two independent helium ions from the residual gas were subtracted. The error resulting from this background subtraction is small in comparison with errors discussed above (± 0.4 neV).

Binding-Energy Derivation. The solution to the Schrödinger equation in the region below a potential barrier is an exponential decay function (Eq. **2**). The helium-dimer binding energy has been extracted from the experimental data by applying an exponential fit to the reconstructed pair-distance distribution (50 a.u. to 300 a.u.). We excluded breakups recorded in the detector plane (with a tolerance of $\pm 33.5^{\circ}$) because indistinguishable background and potentially deadtime effects compromised the data here.

To image the exact shape of the probability density distribution by Coulomb explosion, imaging the ionization probability has to be independent of the internuclear distance. Two consecutive tunnel ionization steps can be influenced by enhanced ionization (24), an effect that depends on the internuclear distance. The steep rise of the probability density at the inner turning point is not very sensitive to this effect and could consequently be imaged by our experiment with an 800-nm laser pulse, which has superior statistics compared with the FEL experiment (Fig. 2). For the exponential region of the probability density, we aim for a high-precision determination of the slope. We therefore used photons from the FEL FLASH to ionize both atoms of the dimer by single-photon absorption. Compared with an 800-nm laser pulse, this ionization process has the additional advantage that the electron energy, and thus the recoil of the electrons onto the nuclei, is much better controlled and has an upper threshold.

Electron-Recoil Correction. The initial ion energy during the Coulomb breakup has to be either zero or well-defined, because Eq. **1** assumes that the KER only results from the potential energy between the two point charges and that there is no additional energy from other sources. The two most important sources of such additional energy are the zero-point kinetic energy from the bound state before ionization and the energy transferred during the ionization process by recoil of the escaping electron.

The first source is negligible for He_2, because the depth of the potential well is only 1 meV. We have also confirmed this finding by calculating the Coulomb explosion quantum mechanically. We found no difference in the KER between the classical calculation using Eq. **1** and the quantum calculation, which automatically includes the initial state zero-point motion (25).

The energy transferred to the two nuclei during the ionization process by the FEL is given by the recoil of the two electrons. The sum momentum distribution of two electrons with a kinetic energy of $E_\gamma - I_P = 42.4$ eV each was calculated and is reflected in the measured data. For two independent ionization events, the distributions of the sum momenta and the momentum difference of the electrons are equal. Although the sum momentum cancels out in the KER calculation, the relative momentum adds to it and increases the measured KER. Correcting this effect reduces the slope of the exponential decaying function by 12.1 neV. Taking this reduction into account, we obtain a binding-energy value of 151.9 neV ± 1.7(stat) ± 10.2(calib) ± 1.4(corr) neV from our experiment. The statistical error is the error of the fit caused by the statistics of the data points, the calibration error is the uncertainty of the calibration of our COLTRIMS reaction microscope, as discussed above, and the error labeled (corr) is the estimated error on the correction procedure compensating the detector efficiency and subtraction of random coincidences.

Comparison with Theory. The exact value of the helium-dimer binding energy was the subject of dispute for decades. Fig. 4 displays the evolution of theoretical predictions as small effects such as deviation from the Born–Oppenheimer Approximation, retardation and quantum, electrodynamical effects were included in calculations and more computational power became accessible. Our measurement is in good agreement with the most recent calculations from Przybytek et al. (5) but cannot distinguish between that and several older calculations (20, 21). Our obtained results on the He_2 wavefunction and binding energy provide an experimental benchmark for theoretical calculations.

ACKNOWLEDGMENTS. We are grateful for excellent support by the staff of FLASH during our beam time. We thank R. Gentry and M. Przybytek for providing their theoretical results in numerical form. The experimental work was supported by a Reinhart Koselleck project of the Deutsche Forschungsgemeinschaft.

1. Riisager K (1994) Nuclear halo states. *Rev Mod Phys* 66(3):1105–1116.
2. Jensen AS, Riisager K, Fedorov DV, Garrido E (2004) Structure and reaction of quantum halos. *Rev Mod Phys* 76(1):215–261.
3. Hansen PG, Tostevin JA (2003) Direct reactions with exotic nuclei. *Annu Rev Nucl Part Sci* 53:219–261.
4. Tanihata I (1996) Neutron halo nuclei. *J Phys G Nucl Part Phys* 22:157–198.
5. Przybytek M, et al. (2010) Relativistic and quantum electrodynamics effects in the helium pair potential. *Phys Rev Lett* 104(18):183003.
6. Schöllkopf W, Toennies JP (1994) Nondestructive mass selection of small van der Waals cluster. *Science* 266(5189):1345–1348.
7. Luo F, McBane GC, Kim G, Giese FC, Gentry WR (1993) The weakest bond: Experimental observation of helium dimer. *J Chem Phys* 98(4):3564–3567.
8. Grisenti RE, et al. (2000) Determination of the bond length and binding energy of the helium dimer by diffraction from a transmission grating. *Phys Rev Lett* 85(11): 2284–2287.
9. Lin H, et al. (2013) Improved determination of the Boltzmann constant using a single fixed-length cylindrical cavity. *Metrologia* 50:417–432.
10. Luo F, Giese CF, Gentry WR (1996) Direct measurement of the size of the helium dimer. *J Chem Phys* 104(3):1151–1154.
11. Cencek W, et al. (2012) Effects of adiabatic, relativistic, and quantum electrodynamics interactions on the pair potential and thermophysical properties of helium. *J Chem Phys* 136(22):224303.
12. Jagutzki O, et al. (2002) Multiple hit readout of a microchannel plate detector with a three-layer delay-line anode. *IEEE Trans Nucl Sci* 49(5):2477–2483.
13. Ullrich J, et al. (2003) Recoil-ion and electron momentum spectroscopy: Reaction-microscopes. *Rep Prog Phys* 66:1463–1545.
14. Jahnke T, et al. (2004) Multicoincidence studies of photon and auger electrons from fixed-in-space molecules using the COLTRIMS technique. *J Electron Spectros Relat Phenom* 141:229–238.
15. Luo F, Kim G, McBane GC, Giese FC, Gentry WR (1993) Influence of the retardation on the vibrational wave function and binding energy of the helium dimer. *J Chem Phys* 98(12):9687–9890.
16. Kunitski M, et al. (2015) Observation of the Efimov state of the helium trimer. *Science* 348(6234):551–555.

17. Aziz RA, Nain VPS, Carley JS, Taylor WL, McConville GT (1979) An accurate intermolecular potential for helium. *J Chem Phys* 70(9):4330–4342.
18. Feltgen R, Kirst H, Köhler KA, Pauly H, Torello F (1982) Unique determination of the He_2 ground state potential from experiment by use of a reliable potential model. *J Chem Phys* 76(5):2360–2378.
19. Tang KT, Toennies JP, Yiu CL (1995) Accurate analytical He-He van der Waals potential based on perturbation theory. *Phys Rev Lett* 74(9):1546–1549.
20. Gdanitz RJ (2001) Accurately solving the electronic Schrödinger equation of atoms and molecules using explicitly correlated (r_{12-})MR-CI. VI. The helium dimer (He_2) revisited. *Mol Phys* 99(11):923–930.
21. Janzen AR, Aziz RA (1997) An accurate potential energy curve for helium based on ab initio calculations. *J Chem Phys* 107(3):914–919.
22. Aziz RA, Slaman MJ (1991) An examination of ab initio results for the helium potential energy curve. *J Chem Phys* 94(12):8047–8053.
23. Lundqvist M, Edvardsson D, Baltzer P, Wannberg B (1996) Doppler-free kinetic energy release spectrum of N_2^{2+}. *J Phys B Atom Mol Opt Phys* 29:1489–1499.
24. Wu J, et al. (2013) Strong field multiple ionization as a route to electron dynamics in a van der Waals cluster. *Phys Rev Lett* 111(8):083003.
25. Schmidt LPhH, et al. (2012) Spatial imaging of the H_2^+ vibrational wave function at the quantum limit. *Phys Rev Lett* 108(7):073202.
26. Tang KT, Toennies JP (1984) An improved simple model for the van der Waals potential based on universal damping functions for the dispersion coefficients. *J Chem Phys* 80(8):3726–3741.
27. Aziz RA, McCourt FRW, Wong CCK (1987) A new determination of the ground state interatomic potential for He_2. *Mol Phys* 61(6):1487–1511.
28. Aziz RA, Slaman MJ (1990) An analysis of the ITS-90 relations for the non-ideality of ^{3}He and ^{4}He: Recommended relations based on a new interatomic potential for helium. *Metrologia* 27:211–219.
29. Aziz RA, Janzen AR, Moldover MR (1995) Ab initio calculations for helium: A standard for transport property measurements. *Phys Rev Lett* 74(9):1586–1589.
30. Korona T, Williams HL, Bukowski R, Jeziorski B, Szalewicz K (1997) Helium dimer potential from symmetry-adapted perturbation theory calculations using large Gaussian geminal and orbital basis sets. *J Chem Phys* 106(12):5109–5122.
31. Jeziorska M, Cencek W, Patkowski K, Jeziorski B, Szalewicz K (2007) Pair potential for helium from symmetry-adapted perturbation theory calculations and from supermolecular data. *J Chem Phys* 127(12):124303.